Chemical Geology 440 (2016) 101–114

Contents lists available at ScienceDirect

Chemical Geology

journal homepage: www.elsevier.com/locate/chemgeo

Basin redox and primary productivity within the Mesoproterozoic Roper Seaway

Grant M. Cox [a,b,c,*], Amber Jarrett [a], Dianne Edwards [a], Peter W. Crockford [c], Galen P. Halverson [c], Alan S. Collins [d], André Poirier [e], Zheng-Xiang Li [b]

[a] Geoscience Australia, GPO Box 378, Canberra, A.C.T., 2601, Australia
[b] ARC Centre of Excellence for Core to Crust Fluid Systems and The Institute for Geoscience Research, Department of Applied Geology, Curtin University, WA, Australia
[c] Department of Earth and Planetary Sciences/Geotop, McGill University, Montréal, Québec, Canada
[d] Centre for Tectonics Resources and Exploration (TRaX), Dept. of Earth Sciences, The University of Adelaide, Adelaide, S.A. 5005, Australia
[e] Département des sciences de la terre et de l'atmosphère/Geotop, Université du Québec à Montréal, Montréal, Québec, Canada

ARTICLE INFO

Article history:
Received 4 December 2015
Received in revised form 20 June 2016
Accepted 25 June 2016
Available online 5 July 2016

Keywords:
Mesoproterozoic
McArthur Basin
Beetaloo sub-basin
Unconventional shale gas
High primary productivity
Basaltic weathering
Atmospheric oxygen

ABSTRACT

The ca. 1.4 Ga Roper Group of the greater McArthur Basin in northern Australia comprises the sedimentary fill of one of the most extensive Precambrian hydrocarbon-bearing basins preserved in the geological record. It is interpreted to have been deposited in a large epeiric sea known as the Roper Seaway. Trace element data suggest that the redox structure of the basin was a shallow oxic layer overlying deeper suboxic to anoxic waters along with a prominent episode of euxinia. These anoxic and sulfidic conditions, as inferred by Mo, V, and U concentrations (molybdenum, vanadium and uranium), developed due to high organic carbon loading consistent with models that suggest that euxinic conditions cannot develop until the flux of organic matter is significantly greater than the flux of bioavailable iron, which permits sulphate reduction to proceed. Considering the high reactive iron and molybdenum contents of these shales and the requirement for S/Fe ratios > 2 for euxinia to develop, suggests that sufficient atmospheric O_2 was available for oxidative scavenging of S and Mo from the continents. This is further supported by prominent negative cerium anomalies within these shales, indicative of active oxidative redox cycling of cerium. We propose that the high organic matter flux was the result of increased nutrient loading to the Roper Seaway from weathering of the continental hinterland. Data from both major and high-field strength elements (niobium, tantalum, zirconium and, hafnium) together with neodymium isotopes ($^{143}Nd/^{144}Nd$) indicate that a likely mechanism for this enhanced nutrient delivery was a shift in sedimentary provenance to a more primitive (i.e. mafic) precursor lithology. This switch in provenance would have increased phosphorus delivery to the Roper Seaway, contributing to high primary productivity and the onset of euxinia. This dataset and model serve as a basis for understanding the temporal evolution of the deepest sections of the Roper Seaway and finer scale changes in the environment at this time.

1. Introduction

The Mesoproterozoic Era (1.6–1.0 Ga) experienced low atmospheric pO_2 (Lyons et al., 2014; Planavsky et al., 2014; Zhang et al., 2016), generally anoxic deep oceans (Canfield, 1998; Lyons et al., 2009b; Reinhard et al., 2013; Sperling et al., 2015) although oxic deep water has been reported (Sperling et al., 2014), a low abundance of passive margins (Bradley, 2008), a period of reduced continental and oceanic arc volcanism (Cawood and Hawkesworth, 2014), and a relatively warm and stable climate (i.e. no evidence for glaciation; (Condie et al., 2001; Kasting and Ono, 2006). Consequently, the Mesoproterozoic has generally been considered a period of environmental stability within the Earth system, comprising the core of the unfortunately entitled "boring billion" years (1.8–0.8 Ga; (Brasier and Lindsay, 1998; Buick et al., 1995). However, against this backdrop of environmental stasis, this period includes the apparent breakup of the supercontinent Nuna (Ernst et al., 2008; Pisarevsky et al., 2014; Roberts, 2013; Rogers and Santosh, 2002; Zhang et al., 2012), formation of the Rodinian supercontinent (Li et al., 2008) and the first appearance of structurally complex microfossils of likely eukaryotic origin (Javaux et al., 2001, 2004; Zhu et al., 2016).

The ca. 1.4 Ga Velkerri Formation, a black-shale dominated unit within the greater McArthur Basin of northern Australia is a key environmental archive for the early–middle Mesoproterozoic due to its low metamorphic grade (sub-greenschist), exceptional thickness, well-constrained age (Kendall et al., 2009) and large variations in organic carbon content. Previous studies of the Velkerri Formation have been motivated by its hydrocarbon potential (Donnelly and Crick, 1988; Jackson and Raiswell, 1991; Volk et al., 2003; Warren et al.,

* Corresponding author at: Geoscience Australia, GPO Box 378, Canberra, A.C.T. 2601, Australia.
E-mail address: grant.cox@curtin.edu.au (G.M. Cox).

http://dx.doi.org/10.1016/j.chemgeo.2016.06.025

1998), with a focus on source rock characterisation and hydrocarbon generating potential. Prior work has shown that the Velkerri Formation hosts some of the oldest known 'live' hydrocarbon occurrences (Jackson et al., 1986), and continues to generate substantial interest as an unconventional gas play (Munson, 2014). Despite these detailed studies on its source rock potential, the environmental conditions prevailing during the deposition of the Velkerri Formation have not been fully elucidated. A better understanding of the interplay between organic matter production, preservation and environment is essential to developing models for Precambrian petroleum systems.

High total organic carbon (TOC) content within sediments has been attributed to various factors including high primary productivity (Pedersen and Calvert, 1990), warm and wet climatic conditions resulting in high nutrient fluxes (Condie et al., 2001; Meyer and Kump, 2008), the combined effects of climate and palaeogeography creating nutrient traps (Meyer and Kump, 2008), basin redox conditions facilitating enhanced preservation potential (Hartnett et al., 1998), mineralogical controls on preservation potential (Hedges and Keil, 1995; Kennedy et al., 2002; Mayer, 1994) and the relative rate of clastic to biogenic sedimentation (Müller and Suess, 1979). In view of these competing processes, it is easy to envisage that the relative importance of these factors may vary in both time and space. Therefore, an understanding of the principal control on organic carbon burial serves to increase our understanding of both local and global environments and has implications for Mesoproterozoic atmospheric oxygen levels.

Here organic carbon data is coupled with major and trace element geochemistry, neodymium isotopic ratios and high-resolution quantitative mineralogy, in order to discriminate between competing processes that contributed to the formation of the exceptionally organic-rich sediments of the Velkerri Formation. This approach provides a basis for understanding key environmental controls on organic matter production and preservation that can be applied more broadly to assessing Precambrian petroleum systems.

2. Regional geology

2.1. The Roper Group

The Roper Group (Wilton Package of Rawlings, (1999)) of the Northern Territory is younger of the four unconformity-bound sedimentary packages (Fig. 1A) of the McArthur Basin (Jackson et al., 1987; Rawlings, 1999). Previous work has left the Roper Group with variable interpretations with it comprising of three (Warren et al., 1998), five (Powell et al., 1987) to possibly six (Abbott and Sweet, 2000; Jackson et al., 1987) shoaling (coarsening up) sequences forming a thick package (~1–5 km) of dominantly siliciclastic sedimentary rocks preserved

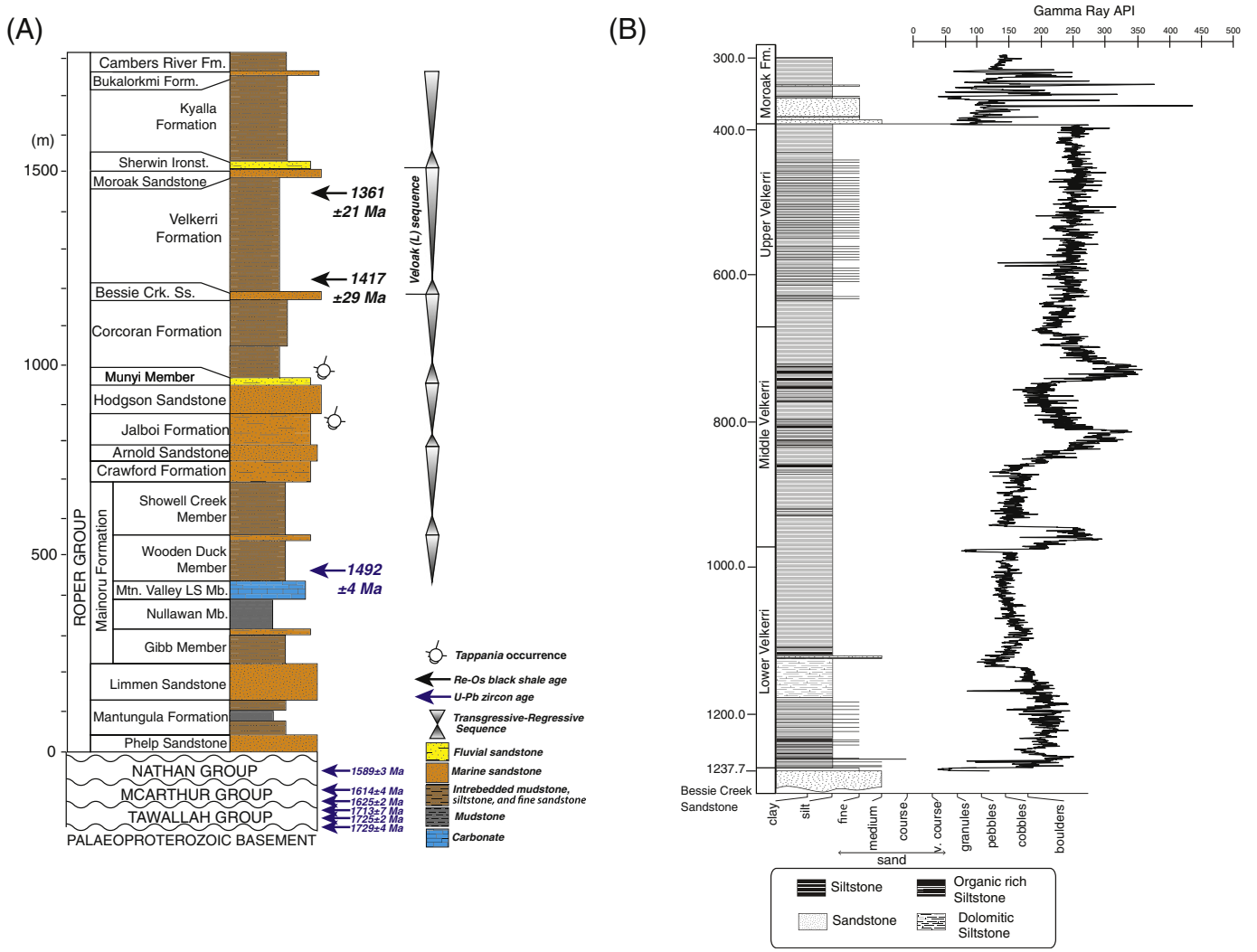

Fig. 1. (A) Simplified stratigraphy of the Roper Group, modified from Abbott et al. (2001), with transgressive–regressive sequences from Jackson et al. (1988) and Abbott and Sweet (2000). Re–Os ages for the Velkerri Formation are from Kendall et al. (2009) while the broader chronostratigraphy is adapted from Brasier and Lindsay (1998) and Southgate et al. (2000). Tappania occurrences are from Javaux et al. (2001). (B) Stratigraphic log of the Altree 2 core.

over ~145,000 km^2 (Abbott and Sweet, 2000; Jackson et al., 1987; Sweet and Jackson, 1986) (Fig. 2).

Significant lateral thickness changes occur within the Roper Group. It is thin (~1–2 km) in the vicinity of the east–west trending Urapunga Fault Zone (the Urapunga Tectonic Ridge of Powell et al. (1987)) (Fig. 2), of moderate thickness over the Broadmere Inversion Structure (Lindsay, 2001) (~2 km), and thinnest (<500 m) over the north-south trending Batten Fault Zone (Fig. 2) (Abbott and Sweet, 2000; Jackson et al., 1987; Plumb and Wellman, 1987; Rawlings et al., 2004). Southwest of the Batten Fault Zone, the Roper Group thickens to >5 km in the Beetaloo Sub-basin (Abbott and Sweet, 2000; Jackson et al., 1987; Plumb and Wellman, 1987; Rawlings et al., 2004) (Fig. 2), which is interpreted to represent the main depocentre of the Roper Seaway (Abbott and Sweet, 2000; Plumb and Wellman, 1987). Thick sections are also present north of the Urapunga Fault Zone (Powell et al., 1987), however, the northerly extent of the Roper Group is less well defined but likely extends offshore under the Arafura Basin (Pietsch et al., 1991; Plumb and Roberts, 1992).

Two contrasting tectonic models have been proposed for the origin of the Roper Seaway. One model suggests that the Roper Group strata were deposited in a shallow-marine to shelf environment that originated as an epicontinental platform in response to lithostatic extension and

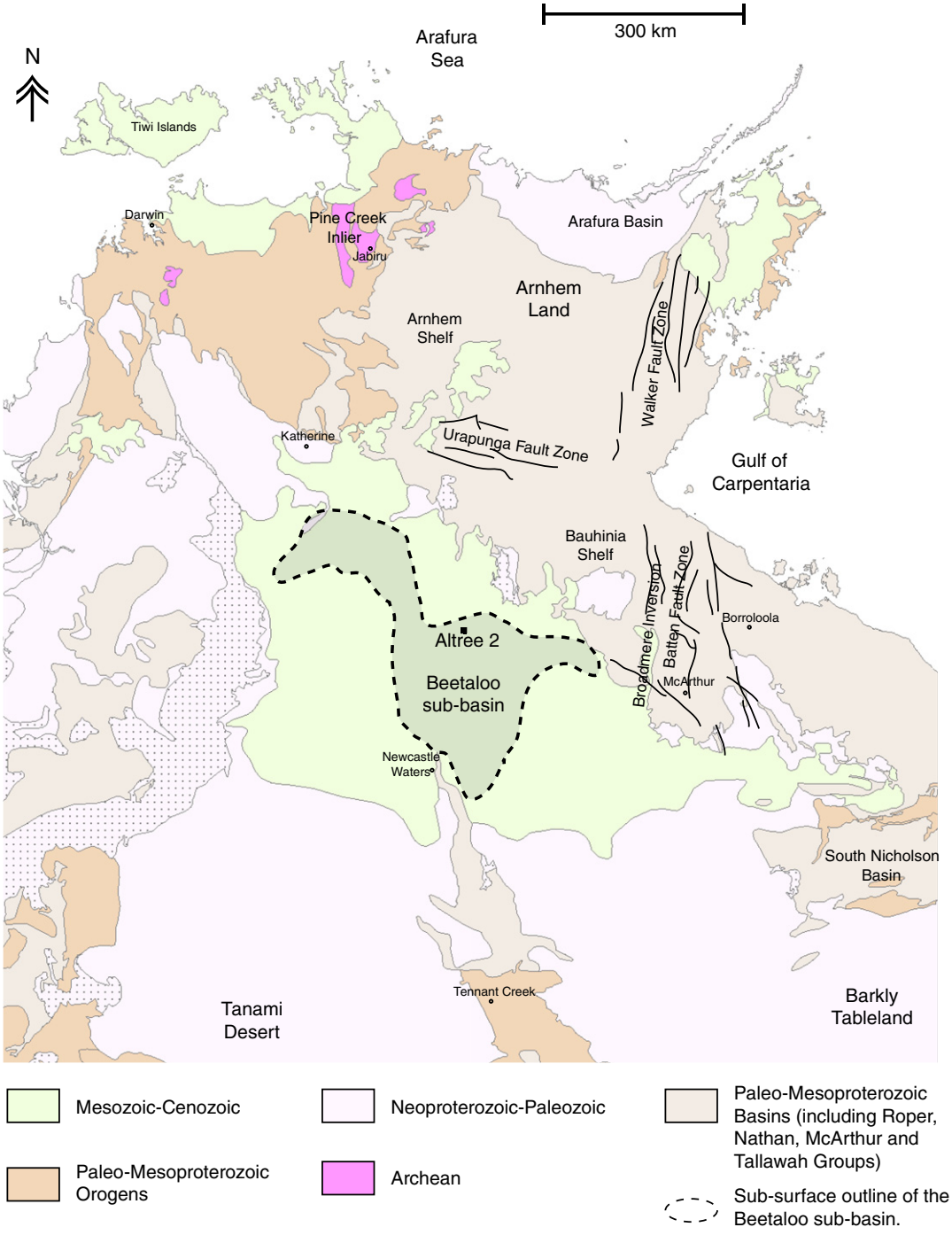

Fig. 2. (A) Map showing the distribution of Paleo-Mesoproterozoic basins of the Northern Territory, Australia. The McArthur Basin is a loose term which includes the Roper, Nathan, McArthur and Tallawah Groups, which range in age from ~1.3 Ga to ~1.8 Ga. Base map was produced using the STRIKE application of the Northern Territory Geological Survey (http://strike.nt.gov.au/). Sub-surface outline of the Beetaloo sub-basin is from Dhu (2015).

sagging (Betts and Giles, 2006; Foster and Ehlers, 1998; Spikings et al., 2001; Spikings et al., 2002). A second model suggests that the Roper Group was deposited on an intracratonic ramp that developed during orogenic flexure (Abbott and Sweet, 2000).

Donnelly and Crick (1988) inferred deposition of the Roper Group within a large lake or silled basin based upon isotopically heavy sulphur values (δ34S + 3.6‰ to + 34.4‰) from disseminated pyrite presented as evidence for a low sulphate environment. In contrast, Jackson and Raiswell (1991), inferred a marine environment based on C–S–Fe systematics in the shales of the Velkerri Formation. Shen et al. (2003) proposed that $\delta 34S_{pyrite}$ values as light as ~− 30‰ reflect inner shelf to basinal gradients in sulphate concentrations in a low sulphate Mesoproterozoic ocean, consistent with data from other Mesoproterozoic basins that imply low marine sulphate concentrations (e.g. Kah et al., 1999). A marine origin is further supported by the wide lateral continuity of the Roper Group (Rawlings, 1999; Rawlings et al., 2004), facies associations and stacking patterns typical for sequence development on a siliciclastic continental shelf, and preserved sedimentary structures typical of open marine deposition such as hummocky and swaley cross-stratification (Abbott and Sweet, 2000).

Correlations between the Roper Group and the South Nicholson Group have been used to infer the existence of a larger 'Roper Superbasin' (Abbott and Sweet, 2000; Jackson et al., 1999). Despite divergence in tectonic interpretations, agreement exists on its intra-cratonic setting and that its deposition is distinct from the underlying sedimentary packages of the greater McArthur Basin.

2.2. The Velkerri Formation

The Velkerri Formation comprises the initial deep water facies of sequence 3 of Warren et al. (1998), sequence L of Jackson et al. (1988) and the Veloak sequence of Abbott et al. (2001) (Fig. 1A) The Veloak sequence comprises dominantly basinal facies, including organic-rich muds and silts transitioning up-section to cross-bedded sandstones of the Moroak Sandstone (Fig. 1B). Abbott et al. (2001) define the top of the sequence as the base of the Sherwin Ironstone (which they regard as the transgressive systems tract of the overlying Shermi sequence) and argue that the Veloak sequence represents mainly a high-stand systems tract above a condensed transgressive systems tract whose base is the top of the underlying Bessie Creek Sandstone. This is observed in the Altree 2 core (Fig. 1B), which forms the basis of this study and was drilled within the Beetaloo Sub-basin (Fig. 2). This core preserves ~930 m of Velkerri Formation mudstones and siltstones, which transition into minor sandstones at the top of the section, where it is unconformably overlain by basaltic lava flows of the Nutwood Downs Volcanics. The formation itself is informally sub-divided into the lower, middle and upper members based upon variations in total organic carbon content (TOC) and gamma ray response (Fig. 1B) (Warren et al., 1998). The detailed sedimentology of the Velkerri Formation has been described by Jackson and Raiswell (1991) and Warren et al. (1998). High resolution X-ray diffraction (XRD) analysis of the fine-grained components (this study) reveals a dominant mineralogy comprising illite, smectite, kaolinite, feldspar, and quartz with minor phases including glauconite, pyrite and carbonate. As discussed in detail later in this contribution, this mineralogy varies systematically up section (Fig. 3).

Two rhenium–osmium (Re–Os) ages of 1417 ± 29 Ma and 1361 ± 21 Ma (Kendall et al., 2009) from the base and top of the Velkerri Formation, respectively, constrain the age of the Veloak sequence between ca. 1420–1360 Ma, but given the error on the ages, do not permit precise constraints on the timescale of Velkerri deposition. These ages are consistent with a Sensitive High Resolution Ion MicroProbe (SHRIMP) U–Pb zircon (tuff) age of 1492 ± 4 Ma from the Mainoru Formation of the lower Roper Group (Southgate et al., 2000).

3. Method summary

Rocks samples were obtained from the Altree 2 drillcore, housed at the Northern Territory core library in Darwin. Samples were collected approximately every 10 m. Samples were washed to be free of surface contamination and crushed to a fine powder in a tungsten carbide mill. X-ray diffraction (XRD) analyses were performed on the raw powder using a Bruker D4™ X-ray diffractometer. Quantification of the multiphase mixtures using Rietveld quantitative analysis was undertaken using the DIFFRAC™ software suite. Major and select trace element abundances were analysed by X-ray fluorescence (XRF) using a Bruker S8 Tiger™ spectrometer. Major elements, chromium (Cr), nickel (Ni) and vanadium (V) were analysed using 30 mm diameter fused beads prepared from a 1:6 sample/lithium tetraborate mixture from calcined powder. The trace elements scandium (Sc), rubidium (Rb), strontium (Sr), zirconium (Zr), niobium (Nb) and yttrium (Y) were analysed using 35 mm diameter pressed pellets prepared at a pressure of 2 t from a mixture of 15 g raw sample powder with 1.6 mL of a PVA/water binder. Trace elements, including rare earth element (REE) analyses, were undertaken via quadrapole inductively coupled plasma mass spectrometry (Q-ICP-MS) using an Agilent 7500 series machine. Solutions for Q-ICP-MS analysis were prepared from the multi-acid dissolution of ~200 mg of the individual fused disks. Ten replicate samples were analysed along with multiple analyses of two international shale standards (SCo-1 and SBC-1 — see Table S2) and a single internal basalt standard (WG1 — see Table S2). Samarium and neodymium (Sm–Nd) analyses were carried out on purified (via chromatography) Sm and Nd solutions after multi-acid digestion of calcined powders. Measurements were made on a Nu Plasma II Multicollector Inductively Coupled Plasma Mass Spectrometer (MC-ICP-MS) and internal mass fractionation was corrected utilising the isotope dilution method. Total organic carbon measurements and Rock-Eval pyrolysis parameters were determined via pyrolysis using ~60 mg of raw sample powder with blanks run every 10 samples on a Rock-Eval 6™ instrument. Rock-Eval pyrolysis data was screened using quality control criteria defined in Hall et al. (2016). Details of these methods can be found in the Supplementary material.

4. Results

4.1. Mineralogy

Major mineral phases for the Velkerri Formation shales include quartz, kaolinite, smectite, K-feldspar, plagioclase and illite, while minor phases include glauconite, pyrite, magnetite and carbonate. While nearly all samples contain this assemblage, systematic changes occur with depth (Fig. 3). Specifically, the abundance of plagioclase declines markedly up section, disappearing (from detection) altogether above ~597 m, which corresponds to a significant increase in kaolinite content. Most samples contain both siderite and dolomite with both being only a minor component of most samples (generally <1%). Two exceptions contain 34% (at 410.55 m) and 42% (at 480.65 m) siderite. Total clay mineral content of all samples varies between 22% and 69%. Based on the black shale series of Stribrny and Urban (1989), the upper Velkerri Formation primarily consists of argillaceous to siliceous shales, the middle Velkerri of argillaceous black shales, while the lower Velkerri are dominantly argillaceous shales with minor intervals of argillaceous black shales.

4.2. Rock-Eval pyrolysis

Total organic carbon (TOC) for the Velkerri Formation shales (Fig. 4A) varies from 0.04% to 8.07% (average = 1.96%, st. dev. = 2.17) with the highest TOC contents confined principally to the middle Velkerri (average = 4.63%, st. dev. = 0.7%). Using the quality control criteria defined in Hall et al. (2016), the majority of samples provide

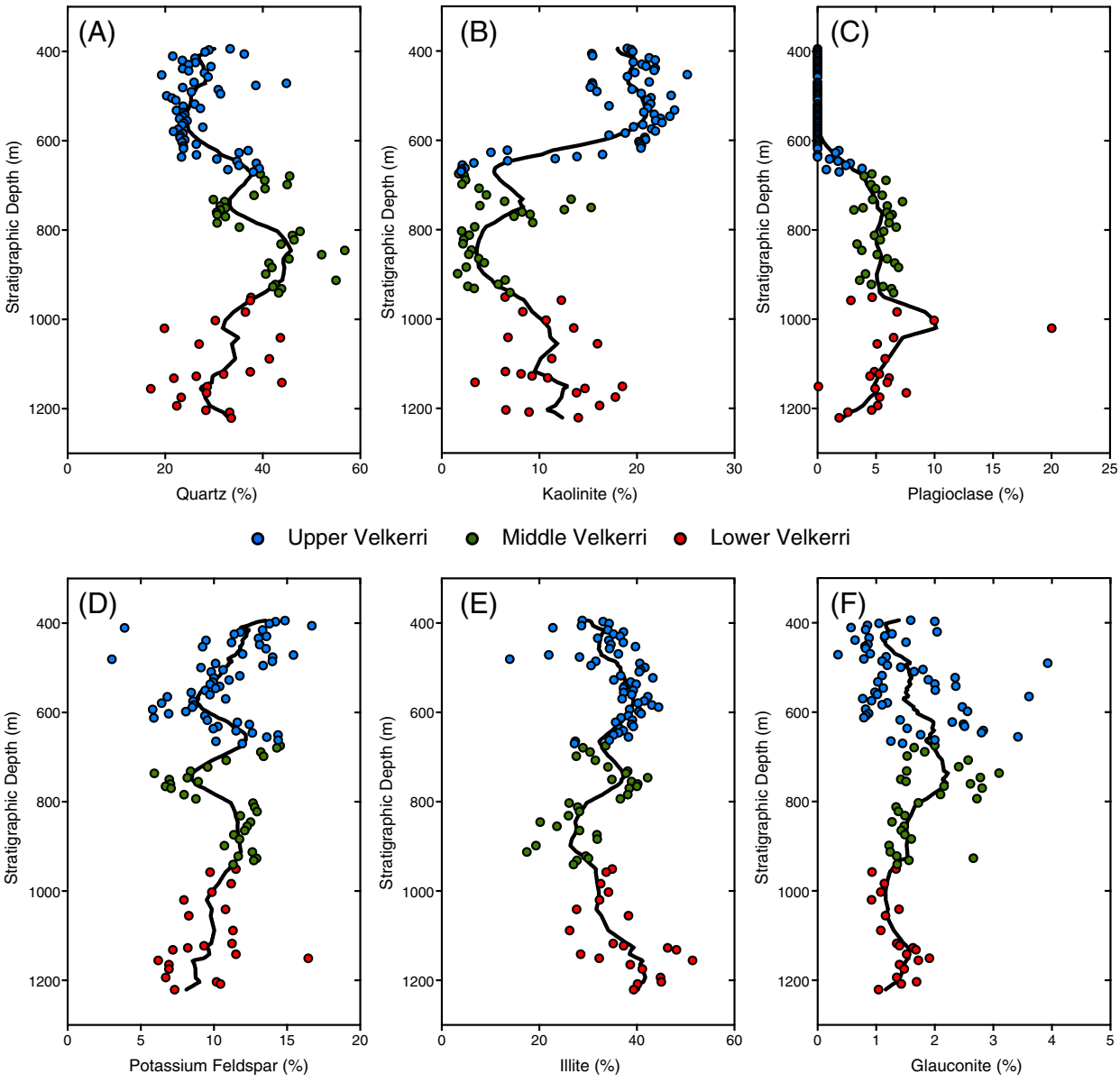

Fig. 3. Variations in sample mineralogy up section through the Velkerri Formation. Thick black line is a 10-point LOWESS non-parametric curve fit.

reliable data while analysis of standard reference material shows the accuracy and precision of the Rock-Eval pyrolysis analyses which were less than one standard deviation (see Table S2). Middle and upper Velkerri samples have low Tmax values indicative of low thermal maturity while values for the lower Velkerri indicate overmaturity. Member averages for Rock-Eval pyrolysis variables are shown in Table 1. Explanation of Rock-Eval pyrolysis variables is listed in Table S1 while the full data set can be found in Table S4 of the Supporting Supplementary material.

4.3. Major and trace elements

Fig. 5 shows stratigraphic variations in selected environmentally sensitive major and trace elements. Fe_T/Al ratios are variable but are higher than that of the Post Archean Australian Shale (PAAS) composite (Fig. 5A) (Taylor and McLennan, 1985). Molybdenum (Mo) exhibits strong up-section variations reaching maximum observed concentrations of nearly 100 ppm within the middle Velkerri (Fig. 5C), whereas Mo/TOC data indicate that Mo concentrations are partially decoupled from TOC (Fig. 5D). Trends for uranium (U) and vanadium (V) are similar to that of Mo (Fig. 5E–H). Phosphorous (P) concentrations are generally found at crustal concentrations (Taylor and McLennan, 1985) within organic-poor shales but are enriched by an order of magnitude in organic-rich shales (Fig. 5B). REE concentrations (Table S6) are typical of shales (i.e. PAAS; (Nance and Taylor, 1976) but variations in calculated cerium anomalies (Ce^*) are present and are observed in organic-rich rich samples (Fig. 5I). No positive Eu anomalies (Eu^*) are evident (Fig. 5J). The full major and trace element dataset can be found in the Supporting Supplementary information (Tables S5 and S6).

4.4. Sm/Nd isotopes

Sm/Nd analysis was undertaken on 28 samples covering the lower, middle and upper Velkerri Formation. Initial $\varepsilon_{Nd(t)}$ varies from primitive values of +0.7 to as evolved as −6.6, whereas initial 147Sm/144Nd values fall within the distinctly crustal range, averaging 0.1254, typical of Proterozoic sediments (Goldstein et al., 1984). Although variations occur between the various members of the Velkerri Formation, averages for each member reveal that the middle Velkerri Formation is the most

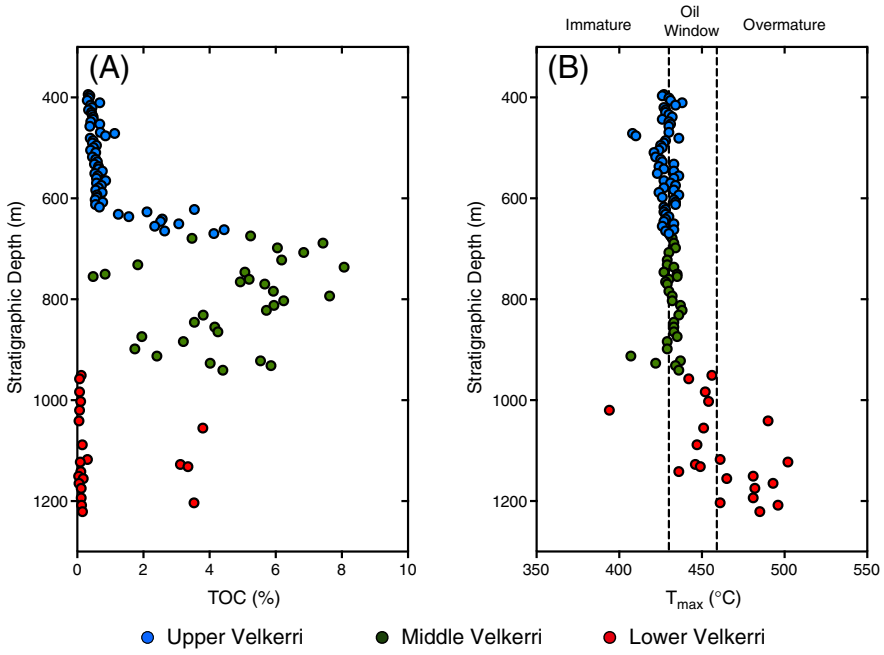

Fig. 4. (A) Up section variations in TOC showing the pronounced TOC enrichment of the middle Velkerri Formation. (B) T_{max} proxy for thermal maturity indicating that upper and middle Velkerri samples have experienced temperatures up to the oil window while lower Velkerri samples have experienced higher temperatures up to and into the gas window.

isotopically primitive member from the perspective of both $\varepsilon_{Nd(t)}$ and 147Sm/144Nd ratios. Full results are detailed in Table 2.

5. Discussion

5.1. Evaluation of total organic matter and source rock potential

Pyrolysis data suggest that variations in thermal maturity (T_{max}) are decoupled from kerogen content (i.e. S2, $r = -0.17$, statistically insignificant at $\alpha = 0.05$) with a small inverse relationship with free hydrocarbon content (S1, $r = -0.21$, statistically significant at $\alpha = 0.05$) (Table 3). A plausible interpretation of this relationship is that very little organic matter has been lost (i.e. by generation and expulsion of hydrocarbons) from the upper and middle Velkerri samples. Consequently, it seems likely that the TOC measured is an accurate reflection of primary organic matter content.

With respect to the upper and middle Velkerri, while they have largely indistinguishable thermal maturity based on invariant T_{max} (Table 1 and Fig. 4), hydrocarbon production (i.e. PI = S1/(S1 + S2)) increases with depth from the upper to middle Velkerri (Fig. 6), this covariation with respect to depth, most likely indicates increasing thermal maturity with burial depth. However, this relationship breaks down at either side of the informal middle–lower Velkerri boundary. The variance exhibited in both TOC and PI for the lower ~200 m to 300 m of the Velkerri Formation, and seen elsewhere in the McArthur Basin (Crick et al., 1988; Warren et al., 1998), is possibly best explained by their increased thermal maturity and variable retention and expulsion of hydrocarbons. This increase in thermal maturity for the lower Velkerri Formation may be simply a function of increased burial depth, alternatively, the presence of proximate dolerite sills in the lower portions of the Altree 2 core may have resulted in post-depositional magmatic heating. The 'live' oil in BMR Urapunga 4 (Jackson et al., 1986) is attributed to transient magmatic heating of organic-rich rocks over a narrow depth/maturity interval (Crick et al., 1988). Considering that dolerite sills are found throughout the McArthur Basin (Abbott et al., 2001), this may be either a regional feature of the Beetaloo Sub-basin or it may apply to the entire extent of the Roper Group.

5.2. Basin redox conditions

5.2.1. Deep water redox

In order to assess basin redox conditions, we have made use of those trace elements that are naturally redox sensitive and exhibit substantial changes in behaviour through the transition from oxic, suboxic, anoxic to euxinic conditions. The elements Mo, V and U have been commonly used for this purpose (e.g. Algeo and Maynard, 2004; Kunzmann et al., 2015; Lyons et al., 2009a; Tribovillard et al., 2006).

Molybdenum (Mo) is a widely used trace metal redox indicator having formed the basis for many prominent redox studies (e.g. Anbar et al., 2007; Scott et al., 2008). Under oxidising conditions Mo is weathered from crustal sulphides and delivered to the marine environment via rivers. Mo occurs as the molybdate ion in seawater (MoO_4^{2-}) and is the most abundant trace metal in the modern ocean (Tribovillard et al., 2006) being present at levels of ~105 nM (Collier, 1985). Its utility as a redox proxy is related to the fact that Mo concentrations are minimally

Table 1
Rock-Eval variables presented as averages for each member of the Velkerri Formation. HI = hydrogen index (HI = 100 * S2 / TOC), OI = oxygen index (OI = 100 * S3 / TOC), TOC = total organic carbon, RC = residual carbon, MINC = mineral carbon, PI = production index (PI = [S1 / (S1 + S2)]). See Table S1 for further explanation of Rock-Eval variables.

Member	S1	S2	S3	Tmax (°C)	HI	OI	TOC	RC	MINC	TPI
Ave. Upper Velkerri	0.34	1.90	0.40	428.43	130.19	67.16	0.97	0.76	0.43	0.12
St. Dev. Upper Velkerri	0.61	3.38	0.48	5.31	82.77	96.58	0.97	0.67	0.64	0.08
Ave. Middle Velkerri	2.10	11.50	0.26	431.23	238.77	8.35	4.63	3.49	0.26	0.19
St. Dev. Middle Velkerri	0.73	6.37	0.10	5.67	72.12	9.42	1.96	1.51	0.52	0.08
Ave. Lower Velkerri	0.22	0.63	0.09	463.05	67.62	63.67	0.75	0.67	0.07	0.11
St. Dev. Lower Velkerri	0.47	1.23	0.06	25.31	30.73	74.46	1.35	1.21	0.11	0.10

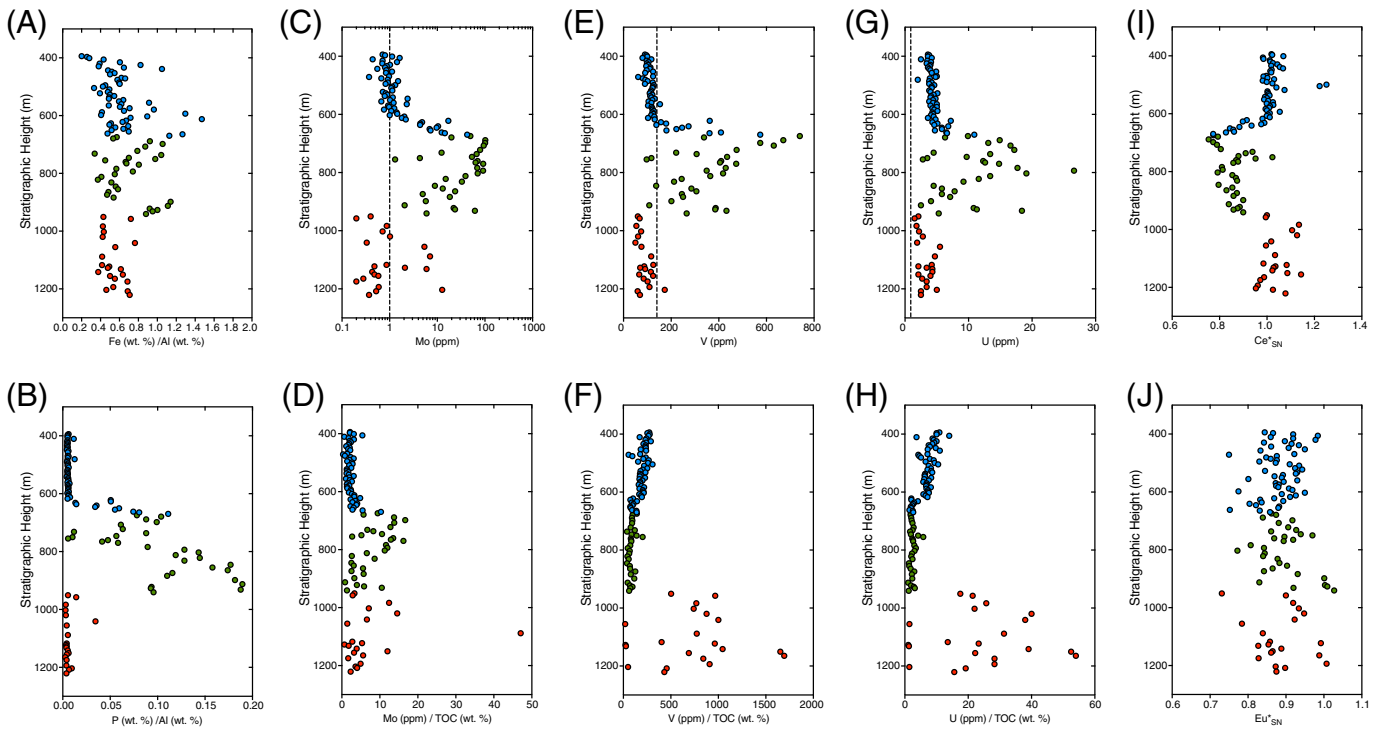

Fig. 5. Selected redox sensitive major and trace element plots element versus stratigraphic height. (A) Fe_T/Al, (B) P/Al, (C) Mo concentrations. (D) Mo/TOC, (E) V concentrations, (F) V/TOC contents, (G) U concentrations, (H) U/TOC contents, (I) Ce anomaly calculated as $Ce^*_{SN} = Ce_{SN} / [0.5(La_{SN} + Pr_{SN})]$ where SN refers to shale normalisation using PAAS. (J) Eu anomaly calculated as $Eu^* = Eu_{SN} / [0.5(Sm_{SN} + Gd_{SN})]$ where SN refers to shale normalisation using PAAS. Solid black lines in (C), (E) and (G) are the composition of the Post Archean Australian Shale (PAAS). Values for PAAS are from Nance and Taylor (1976).

affected by detrital material, it complexes with organic molecules, and it reacts strongly with hydrogen sulphide, such that it is effectively removed from seawater and porewaters under anoxic and sulphidic (i.e. euxinic) conditions. Mo concentrations above background (i.e. crustal and average shale values) occur when it is trapped in shales through the deposition of organo-metallic complexes, where basin anoxia allows for the preservation of organic matter (this still requires hydrogen sulphide of ~10 μM (Erickson and Helz, 2000) to quantitatively form the particle reactive thiomolybdates (Scott and Lyons, 2012), or under euxinic conditions where it can be sequestered in sediments by sulphides. Enrichments are also linked to the global Mo seawater inventory, which is linked to atmospheric O_2 level, consequently, authigenic Mo enrichment requires both an oxidative source of molybdate (Scott et al., 2008) and hydrogen sulphide to be sequested in sediments (Scott and Lyons, 2012).

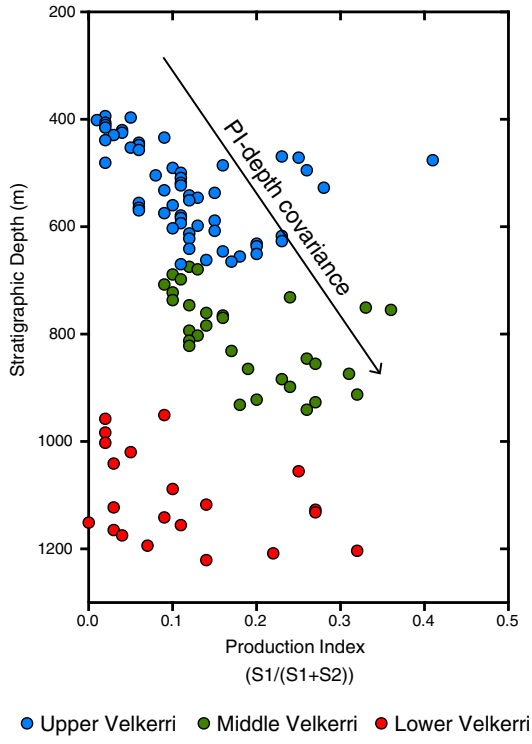

Fig. 6. Variation in Production Index (PI) as a function of depth. PI increases with depth until the lower Velkerri is reached at depths of ~950 m, past this depth no covariance with PI is apparent.

Vanadium is the second most abundant trace metal in modern seawater (~40 nM) (Tribovillard et al., 2006) and also has strong affinities towards organo-metallic complexes (Algeo and Maynard, 2004). Specifically, under oxic conditions, vanadium occurs as V^{5+} as vanadate oxyanions while under anoxic conditions V^{5+} is reduced by both organic compounds and hydrogen sulfide to V^{4+} (Breit and Wanty, 1991). Consequently, while organic matter and authigenic clays (Peacor et al., 2000) are the sinks for V, marked enrichment occurs at both the oxic–anoxic boundary and anoxic–euxinic boundary (Algeo and Maynard, 2004; Tribovillard et al., 2006). Hyper V enrichment is also documented when sulphide levels are high enough so as to allow further reduction of V^{4+} to V^{3+} (Breit and Wanty, 1991; Lewan and Maynard, 1982; Wanty and Goldhaber, 1992).

Uranium also shares some of the above characteristics, and is present in seawater in the oxidised form of U^{6+} but at lower concentrations (~13.4 nM) than Mo and V and is typically bound to dissolved carbonate ions ($UO_2(CO_3)_3^{4-}$); (McManus et al., 2005). Most simply, when oxidised, U is soluble and when reduced it is immobile (Langmuir, 1978). Uranium has a similar redox potential to Fe over a wide range of pH conditions (Barnes and Cochran, 1993; Bruno et al., 1995), but is unaffected by the redox cycling of Fe and Mn complexes. McManus et al. (2005) showed that U inversely correlates with oxygen

penetration depth and is positively correlated with TOC content. This correlation persists under euxinic conditions, revealing the decoupling of U from sulphide phases (Klinkhammer and Palmer, 1991; Tribovillard et al., 2006). Consequently, in a dominantly oxic water column, U enrichment may occur within the sediment below the oxygen penetration depth, however, under mildly anoxic water column, it is reduced to U^{4+} and precipitates as UO_2, U_3O_7, or U_3O_8 (Klinkhammer and Palmer, 1991; Tribovillard et al., 2006). The formation of organo-metallic complexes may speed the transport of U from the water column to sediments (Klinkhammer and Palmer, 1991; McManus et al., 2005; Tribovillard et al., 2006).

In summary, Mo, V and U contents used together, highlight crucial redox controlled variations in their abundances; specifically, Mo and V, show strong linear covariation under anoxic conditions, being removed by organic matter, but undergo further nonlinear enrichment when conditions become euxinic and sulphide sinks become important. U is enriched under both low oxygen and anoxic (sulphidic and ferruginous) conditions (Anderson et al., 1989; Klinkhammer and Palmer, 1991).

Fig. 5 shows that Mo and V are enriched above values typical of the Post Archean Australian Shale (PAAS (Nance and Taylor, 1976)) for the middle Velkerri Formation and some samples of the upper and lower Velkerri Formation, while U is enriched with respect to PAAS throughout the entire formation (Fig. 5G). Correcting for variable dilution by biogenic and authigenic phases (i.e. organic matter, opal, carbonate) through normalisation to Al (Calvert and Pedersen, 1993; Tribovillard et al., 2006) it is evident that trace element (TE) values covary significantly with TOC contents (Fig. 7). This simple linear relationship with TOC content, however, breaks down at both low (~<0.5%) and high (~>4%) values. The mechanistic underpinnings for this relationship have been described by Algeo and Maynard (2004) and Scott and Lyons (2012), where strong linear relationships between TE enrichments and TOC persist under sub-oxic and anoxic conditions where the principal sink for these TEs is organo-metallic complexes. At higher TOC contents, TE enrichments are still ubiquitous, but do not covary linearly with TOC because under these conditions, the presence of water column sulphide, as a sink itself (i.e. for Mo), or in the case of V and U, leading to further reduction and precipitation of reduced V and U species.

This observed pattern in TE enrichment versus TOC content (Fig. 7) suggests pore water enrichment between ~0.5% and ~4% TOC (suboxic to anoxic, non-euxinic; closed system) and water column enrichment above ~4% TOC (euxinic — water column H_2S, open system), and consequently euxinic conditions (Algeo and Maynard, 2004; Scott and Lyons, 2012). In contrast to the middle Velkerri samples, the majority of upper Velkerri samples exhibit strong linear TE covariation with respect to TOC content, consistent with a dominant role for an organic matter sink under suboxic or anoxic conditions (Algeo and Maynard, 2004; Scott and Lyons, 2012).

So far we have limited our discussion of redox to the middle and upper Velkerri Formation, whereas the lower Velkerri Formation samples have variable TE enrichments (Figs. 5 and 7) and show little to no covariance with respect to TOC contents. However, Fe_T/Al ratios reach values as high as ~0.8 (Fig. 5A), Mo concentrations reach values up to maximum of 12 ppm (Fig. 5C), maximum V of ~200 ppm (Fig. 5E), and U is uniformly enriched with respect to typical shale values (Fig. 5G). However, TOC contents in the lower Velkerri Formation appear to have undergone post-depositional changes (Figs. 4 and 6), and consequently the original redox conditions may be somewhat ambiguous. Despite ambiguity in regard to the lower Velkerri member, redox sensitive trace element data are consistent with suboxic to anoxic bottom waters with occasional episodes of euxinia during the deposition of the Velkerri Formation sediments. These episodes of euxinia are most pronounced during deposition of the middle Velkerri and lower parts of the upper Velkerri.

Johnston et al. (2010) suggested that in a low pO_2 environment, and consequently a low nitrate environment, the dominant electron

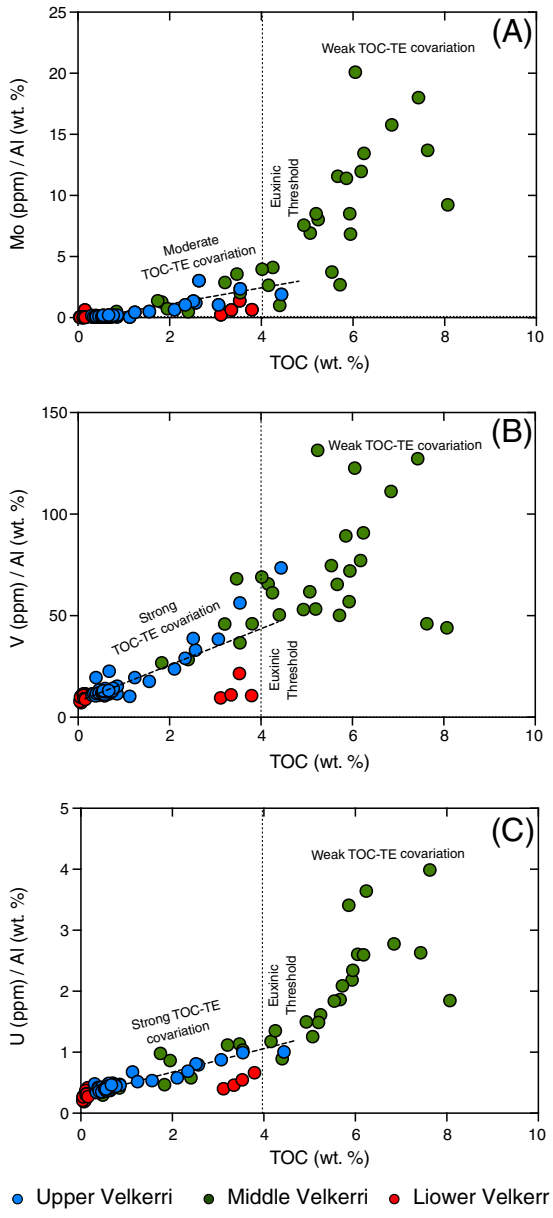

Fig. 7. (A to C) Trace element (TE) enrichments with respect to TOC. Mo, V and U all show similar trends, initial linear covariation with respect to TOC up to ~4% TOC followed by a breakdown of this linear covariation consistent with the onset of intermittent euxinia (Algeo and Maynard, 2004; Lyons et al., 2009a,b). The use of Al normalisation is to correct for authigenic trace element dilutions associated with variable proportions of authigenic mineral and biogenic phases (e.g. carbonate, opal and organic matter) (Calvert and Pedersen, 1993; Tribovillard et al., 2006).

acceptors would be Fe^{3+} and SO_4^{2-}. Taking into account their relative order of reduction (Fe^{3+}, then SO_4^{2-}), Johnston et al. (2010) argued that sulphate reduction should not proceed until all reactive Fe^{3+} had been reduced. Based on stoichiometric relationships, and in anoxic and nitrate poor environments, this would not occur until the flux of organic matter was 4.25 times the flux of reactive Fe^{3+}. Considering the high TOC content of the middle Velkerri samples, it is plausible that this model for euxinic conditions explains the onset of euxinia during this time and that the organic flux exceeded this threshold, allowing for euxinia to develop.

An important implication of this euxinic episode is that euxinia requires S/Fe ratios to exceed 2 and considering that Fe_T/Al ratios (Fig. 5) and the presence of siderite (Table S3) suggest high levels of reactive Fe, very high levels of seawater sulphate would be required for S/Fe ratio > 2. This is combined with the high Mo values recorded by the

middle Velkerri (up to 100× crustal values), also require high levels of seawater Mo (Scott et al., 2008). This combination would seem to require significant levels of atmospheric O_2 (Scott et al., 2008) to supply the necessary Mo and SO_4^{2-} to the water column. Consequently, the results presented provide indirect evidence against the upper pO_2 estimate of <0.1% PAL (Present Atmospheric Level) recently published by Planavsky et al. (2014) and are more consistent with estimates of pO_2 > 4% PAL (Gilleaudeau et al., 2016; Zhang et al., 2016).

5.2.2. Oxygenated surface waters?

Whereas the shales of the Velkerri Formation provide evidence for suboxic to anoxic bottom waters with occasional episodes of euxinia, they also display negative cerium anomalies (Ce*), which are typically associated with an oxygenated water column. In the modern ocean, seawater contains a prominent negative Ce* with respect to bulk earth (Elderfield et al., 1981). This relative depletion in Ce results from the oxidation of Ce^{3+} to Ce^{4+} and incorporation into ferromanganese nodules (Elderfield and Greaves, 1981; Nagender Nath et al., 1994), which conversely preserve positive Ce*. Thus Ce anomalies are sensitive to the redox state of the water column, because under oxic conditions, it is preferentially converted to Ce^{4+} and removed from seawater, whereas under anoxic conditions, it should behave like its neighboring REEs.

To discriminate against the effect of positive La anomalies, we have used the method of Bau and Dulski (1996) to define true negative Ce* (Fig. 8). The Velkerri shales define a coherent array into the field of unambiguous negative Ce anomalies, having values for both Ce* and Pr* that fall well away from unity (Fig. 8).

Although interpretation of the Ce data is complicated by the influence of the detrital component to these sediments (i.e. with REE compositions similar to PAAS), the variations in Ce* apparent in Fig. 8 suggest at the very least, active Ce redox cycling in the Roper Seaway. Furthermore, if it is assumed that the few samples with a positive Ce* are a result of local Ce cycling under suboxic to anoxic conditions (Slack et al., 2007), the array of Ce* and Pr* data is broadly consistent with mixing between an end member with no Ce* and a component that carries an authigenic signature. The relationship between Ce* and TOC content (Fig. 9) indicates that the negative Ce* is limited to those samples with TOC values greater than ~2%, whereas those with low TOC values have no negative Ce anomaly. This pattern suggests that the negative Ce* is carried by organic matter.

Negative Ce* hosted in the organic matter content of black shales has been interpreted to represent an authigenic imprint of oxygenated seawater (Dumoulin et al., 2011; Pi et al., 2013; Slack et al., 2015).

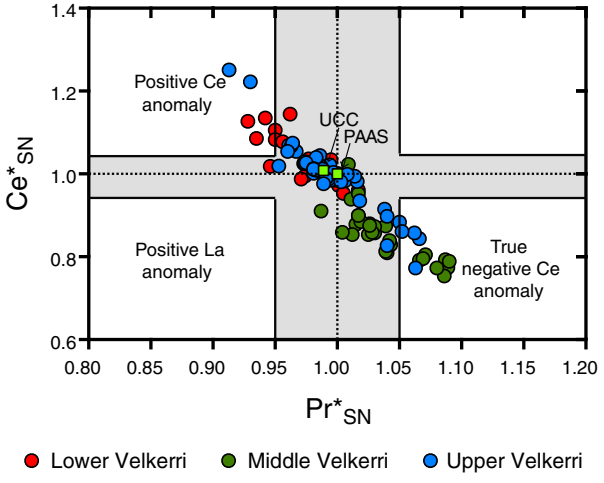

Fig. 8. Shale normalised Ce and Pr anomalies cross plot after Bau and Dulski (1996). $Ce^*SN = Ce_{SN} / 0.5[La_{SN} + Pr_{SN}]$, $Pr^*_{SN} = Pr_{SN} / 0.5[Ce_{SN} + Nd_{SN}]$. Normalization was to the Post Archean Australian Shale (PAAS) (Nance and Taylor, 1976). Values for the Upper Continental Crust (UCC) are from Taylor and McLennan (1995).

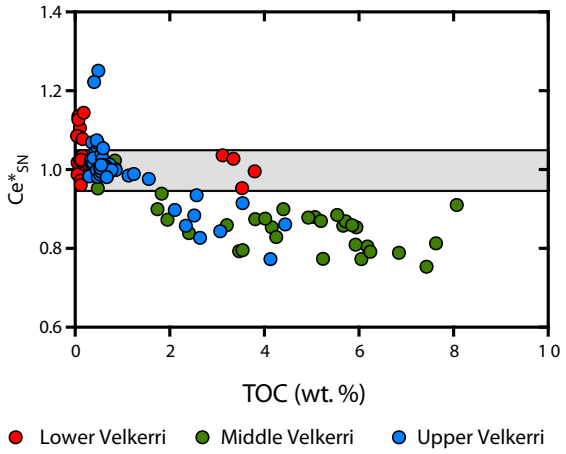

Fig. 9. Shale-normalised (SN) Ce anomaly vs. TOC. Shales with low TOC have a REE budget dominated by siliciclastic material, and so contain no Ce negative anomaly. Negative Ce anomalies are restricted to shales with greater than ~2% TOC, implying that the anomaly is carried by the organic matter.

Considering that negative Ce* is generated in oxic seawater and recorded by authigenic minerals precipitated from seawater, the negative Ce* in the Velkerri shales most likely records highly productive zones within the surface mixed layer of the Roper Seaway. Once again, these results provide indirect evidence against an upper pO_2 estimate of <0.1% PAL (Planavsky et al., 2014).

Shen et al. (2003) independently argued for a redox stratified Roper Seaway, with a shallow oxic layer and anoxic deep waters based on sulphur isotope and iron speciation data. Furthermore, hematite oolitic iron formation is present within the Roper Group (Sherwin Iron Formation; Fig. 1A). Whereas ferrous iron may be oxidized by either oxygenic or anoxygenic pathways (Bekker et al., 2010), the presence of negative Ce* in the black shales analysed herein, favors the former, either in microenvironments rich in cyanobacterially-generated O_2 or, more broadly under oxic conditions in shallow waters.

5.3. Controls on organic matter: climate, sediment provenance and basin redox?

Whereas basin redox conditions may strongly influence organic matter preservation (i.e. Hartnett et al. (1998)), the observation that suboxic to anoxic and euxinic conditions persisted throughout much of the deposition of the Velkerri Formation, suggests that other factors contributed to the variations observed in TOC content. Here we explore two possible extrinsic controls on primary productivity and organic carbon burial in the Roper Seaway; climate and nutrient delivery.

Changes in bulk rock mineralogy and bulk rock chemistry of shales are sensitive to both climate and changes in sediment provenance. Nesbitt and Young (1982) introduced the Chemical Index of Alteration ($CIA = [Al_2O_3] / [Al_2O_3 + CaO^* + Na_2O + K_2O] \times 100$ in molar quantities) and determined that the CIA in shales scaled directly with the intensity of chemical weathering, because more heavily weathered source rocks should be more Al_2O_3-rich. As chemical weathering is strongly affected by climate, they argued that the CIA could be used as a climate proxy where high values indicate warm and wet conditions in the sedimentary catchment, whereas low values indicate dry and cool conditions. This prediction, often corroborated by quantitative mineralogy, has been borne out in numerous studies (Colin et al., 2006; Fagel, 2007; Gingele et al., 1998; Schneider et al., 1997).

Due to the influence of climate on the intensity of chemical weathering and hence on bulk sediment geochemistry, changes in climate can drive changes in nutrient delivery to the oceans, and thus impact primary productivity. In short, intense weathering, so long as accompanied by a regular supply of new material, should increase

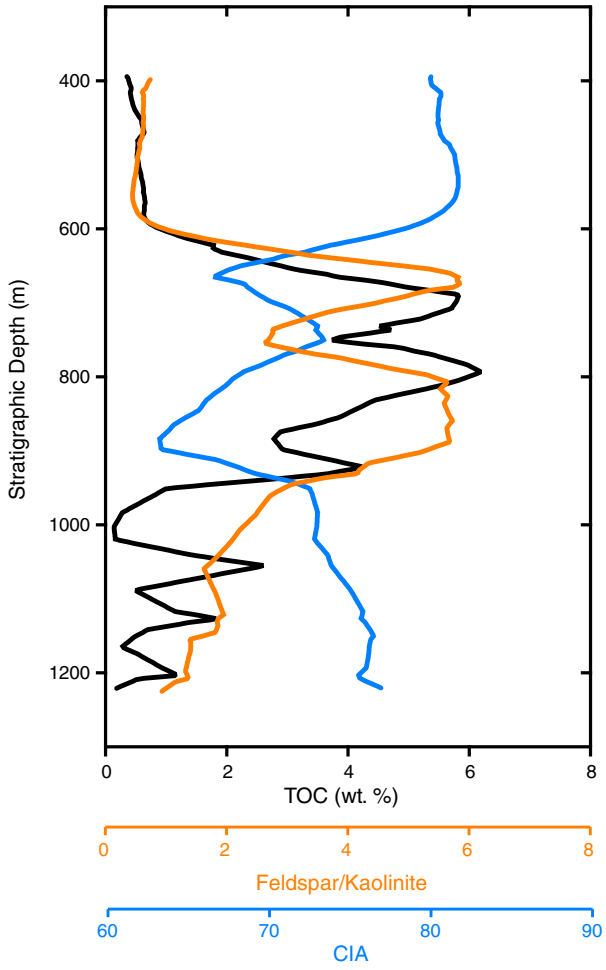

Fig. 10. Covariation of LOWESS-smoothed TOC, Feldspar/Kaolinite ratios and CIA. Variations in CIA and Feldspar/Kaolinite can be interpreted as representing varying degrees of chemical weathering, which is often viewed as a proxy for climate. Alternatively, such change may reflect changes in sediment sourcing. In either case the strong covariation of these variables, especially through the upper 600 m of the formation may suggest a relationship between these changes and the high TOC values of the middle Velkerri Formation. The distinct lack of covariation observed in the lower 200 m may be due to the higher thermal maturity of these samples having undergone post-depositional loss of organic matter (Figs. 4B and 6).

nutrient fluxes. Stratigraphic variations in TOC content, feldspar/kaolinite ratios and CIA through the Velkerri Formation appear to confirm such a relationship (Fig. 10); TOC and feldspar/kaolinite ratios are

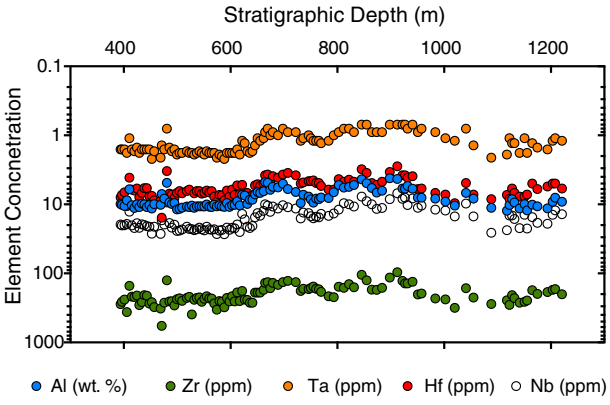

Fig. 11. Covariation of Al, Zr, Ta, Hf and Nb. As Al is supplied overwhelmingly by the detrital fraction of shales, such covariation implies that the HFSE are also hosted by the detrital fraction of these shales.

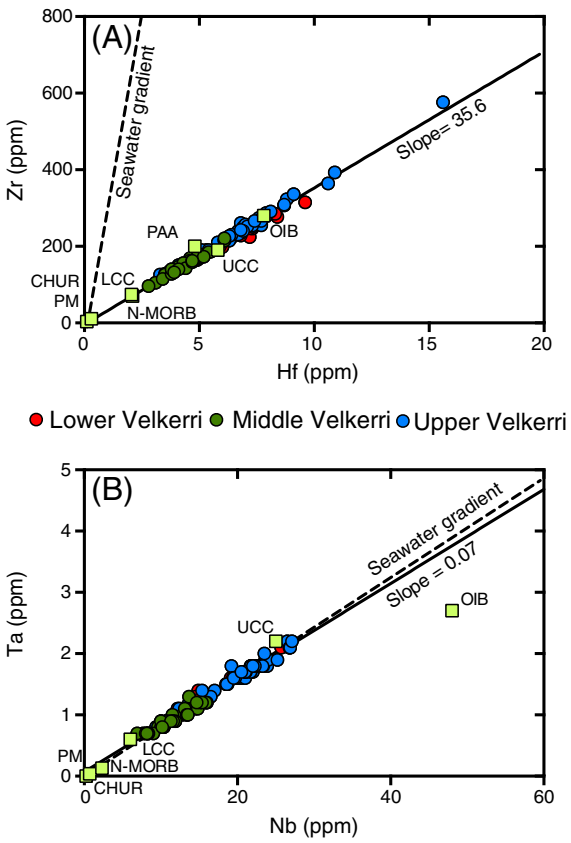

Fig. 12. (A) Zr vs. Hf. (B) Ta vs. Nb. In both (A) and (B) it is evident that the variations recorded in HFSE vary according to natural variations observed in the silicate earth providing a basis to conclude that the HFSE are recording compositional variations in the detrital fraction of the shales. Values for silicate reservoirs are from Sun and McDonough (1989). Gradient for seawater (dashed line) are from Firdaus et al. (2011). UCC = upper continental crust, LCC = lower continental crust, PM = primitive mantle, N-MORB = mid ocean ridge basalt, OIB = ocean island basalt, CHUR = bulk Earth.

strongly positively correlated ($r = 0.87$), whereas TOC and CIA are strongly but inversely correlated ($r = -0.79$).

A *prima facie* interpretation of the coupled feldspar/kaolinite ratios and CIA data is that the middle Velkerri shales record a shift to less intense chemical weathering, presumably due to the onset of a cooler and drier climate. However, high TOC levels during the low CIA interval

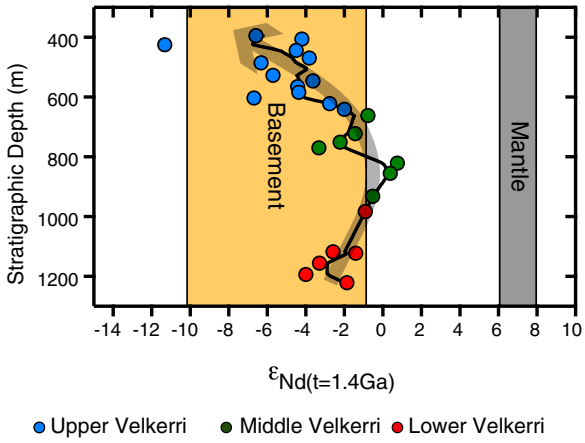

Fig. 13. Up section variations in εNd(t) recorded in the Velkerri Formation. Mantle values (grey zone) are based on Goldstein et al. (1984) while basement values (yellow zone) are from the Arunta Inlier (Sun et al., 1995; Zhao and McCulloch, 1995). Thick black line is a 10-point LOWESS non-parametric curve fit. All $\varepsilon_{Nd(t)}$ values are calculated at 1.4 Ga. See Table S7 for full results.

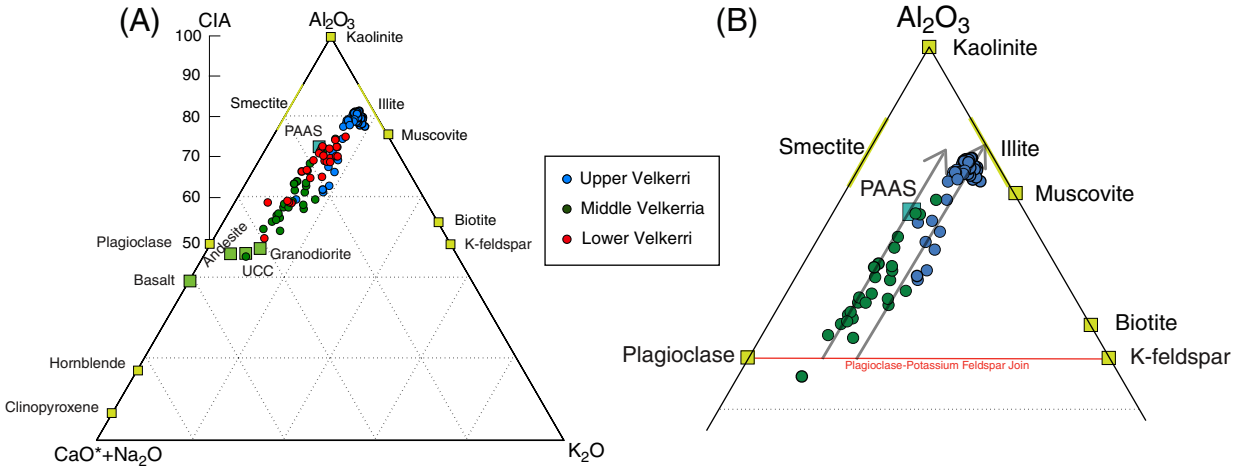

Fig. 14. (A) Chemical weathering ternary after Taylor and McLennan (1995) showing what could be interpreted as a chemical weathering trend. (B) Enlarged version of (A) showing that the middle Velkerri shales are offset from the upper Velkerri shales, such an offset is not possible from a chemical weathering perspective but could be achieved if they are of different sedimentary provenance. Grey arrows show the direction of increased chemical weathering.

are unusual given that cooler conditions and lower release of nutrients should impede primary productivity and organic carbon burial. This paradox could be resolved if the changes in mineralogy and whole rock geochemistry, at least in part, reflect changes in sedimentary provenance rather than climate alone. To evaluate the contribution of source rock variations to the CIA signal, we examine high field strength elements (HFSE) of Nb, Hf, Ta and Zr which tend to be depleted in mafic versus felsic rocks (Sun and McDonough, 1989; Taylor and McLennan, 1995). The HFSE are largely redox-insensitive (Takeno, 2005), have no known biological function, have extremely low aqueous solubilities (i.e. pM; (Firdaus et al., 2011)), and are largely immune to secondary alteration. Consequently, HFSE concentrations in shales should be primarily determined by the siliciclastic fraction, as seen in their covariation with Al (Fig. 11). Furthermore, HFSE cross plots clearly lie along the mantle-continental crust array (Fig. 12), which is distinct from the HFSE Zr–Hf array in seawater (Fig. 12A) (Firdaus et al., 2011). It is evident that the middle Velkerri shales have more primitive HFSE compositions than either the lower or upper Velkerri shales (Fig. 12).

Evidence for a more primitive source to the middle Velkerri shales is also apparent in the Sm/Nd isotopic variations. While the sampling

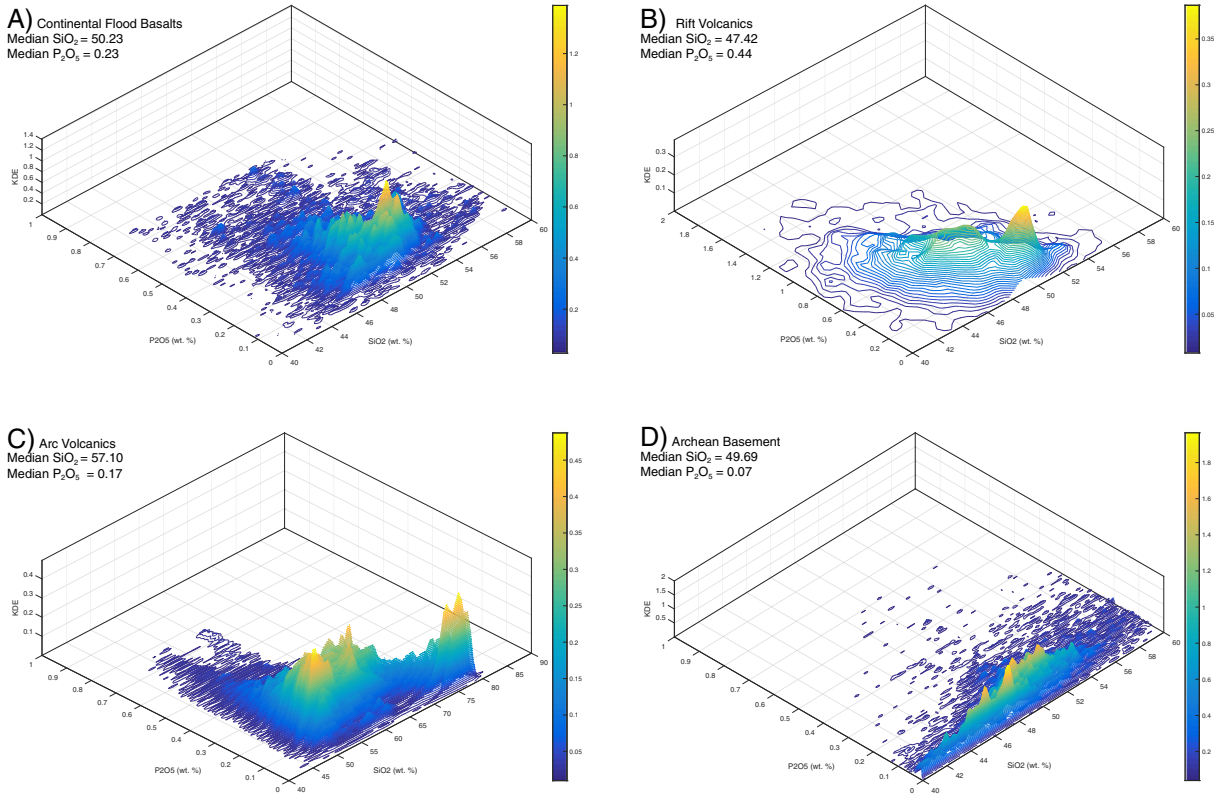

Fig. 15. Phosphorus in igneous rocks. X and Y axis are in weight percent oxide while the Z axis is the Kernel Density Estimate (KDE) which is a measure of data density/probability. (A) continental flood basalt (CFB), (B) rift volcanics, (C) arc volcanics and (D) Archean basement. Clearly evident from all datasets is that P_2O_5 is most enriched for basaltic compositions and depleted in felsic compositions. Data is from the GEOROC repository (http://georoc.mpch-mainz.gwdg.de/georoc/Start.asp).
Modified from Cox et al. (2016).

resolution is coarser, $\varepsilon_{Nd(t)}$ variations show a clear shift to more primitive compositions for the middle Velkerri samples (Fig. 13). This isotopic shift, when considered in conjunction with the primitive HFSE compositions, is hard to reconcile with anything other than a more mafic provenance for the middle Velkerri Formation.

The CIA values from the Velkerri Formation need to be viewed against the backdrop of a shift in provenance, which would strongly alter bulk chemistry. Major element CN–K–Al ternary plots (Fig. 14), while showing a typical chemical weathering trend (Taylor and McLennan, 1995) towards Al_2O_3-rich compositions, also reveal that the middle Velkerri is less chemically weathered, having distinctly lower CIA values (Fig. 14A). Critically, however, middle Velkerri samples are also offset towards the $CaO–Na_2O–Al_2O_3$ join (Fig. 14B), intersecting the plagioclase-potassium feldspar join at more plagioclase rich compositions, indicative of differing provenance (Fedo et al., 1995). As the slopes of the two trends (Fig. 14B) are the same, increased potassic alteration of clays cannot explain this observation, as potassic alteration of clays from a common source terrain results in differing slopes but identical intercepts along the plagioclase-potassium feldspar join (Fedo et al., 1995). Furthermore, if this offset was due to authigenic K-feldspar formation (alteration of plagioclase to potassium feldspar) we would expect to see strong negative covariation between plagioclase and potassium feldspar, especially for the middle and upper Velkerri, such a trend is not observed (Fig. 3). This does not preclude potassic alteration, but does imply that it is not a major driver of major element variations. Consequently, major element data is consistent with a more primitive provenance contribution for the middle Velkerri, as supported by HSFE and Nd isotope data.

5.4. A mafic nutrient pump

While it has been determined that changes in climate (i.e. warmer and wetter conditions) can result in an increase in the nutrient flux supplied to sedimentary basins, the same can be achieved when sediment provenance changes to a more primitive (i.e. mafic) composition due to the relative phosphorus enrichment of mafic lithologies (Fig. 15). Such a scenario has been proposed for the Neoproterozoic through the preferential weathering of contemporary Large Igneous Provinces (LIP) (Cox et al., 2016; Horton, 2015; Rooney et al., 2014). A mafic nutrient pump driven by the weathering of continental mafic lithologies is supported by large compilations of Continental Flood Basalt (CFB) (Fig. 15A), rift volcanics (Fig. 15B), continental arc (Fig. 15C) and Archean basement (Fig. 15D) data. These data highlight that a switch to the weathering of rocks with a more primitive composition has the potential to increase phosphorous delivery to sedimentary basins. This flux would be pronounced for CFB's (Cox et al., 2016; Horton, 2015), but would also be apparent for most continental mafic lithologies (Fig. 16). Increased nutrient delivery would be further enhanced by the ~10× greater weatherability of mafic lithologies over their felsic counterparts (White and Brantley, 1995), potentially offsetting any switch to a colder and drier climate, which is suggested by the CIA data (Figs. 10 and 14). Assuming that phosphorus is the limiting nutrient on geological timescales (Tyrrell, 1999), an increase in mafic provenance, as evinced by HFSE (Fig. 12), $\varepsilon_{Nd(t)}$ (Fig. 13) and major elements (Fig. 14), may help account for the high organic content of the middle Velkerri shales, reconciling the increased TOC content with a climate signal suggesting cooler and drier conditions.

5.5. Implications for continental reconstructions

Variations in the isotopic composition of fine-grained sediments, in particular, variations towards more primitive signatures, have been used previously to constrain the extent of eroded flood basalt provinces (Barovich and Foden, 2000; Cox et al., 2016). While there is no direct evidence for contemporary emplacement of continental basalts within the Roper Group during deposition of the Velkerri Formation (Abbott et al., 2001; Ernst et al., 2008), rifting of the North Australian Craton (NAC) from Laurentia has been proposed at ~1380 Ma (Betts and Giles, 2006; Mulder et al., 2015; Pisarevsky et al., 2014). Possible Australian source terranes include the ~1600 Ma mafic granulites of the Yambo Metamorphic Group (Blewett and Black, 1998; Blewett et al., 1998) and similar aged mafic magmas associated with the Holroyd Group, Savannah Province (Blewett et al., 1997). Non-Australian source terranes that are coincident with ~1380 Ma rifting include the Hart River sills and dykes of northwestern Laurentia ($1380 + 5.3/-3.7$ Ma; (Abbott, 1997; Thorkelson et al., 2005). While this link between Laurentian volcanism and source provenance for the Roper basin is speculative, it is consistent with the available age constraints for deposition of the Velkerri Formation of 1417 ± 29 Ma and 1361 ± 21 Ma (Kendall et al., 2009).

6. Conclusion

Our new dataset provides a temporal record of the deep-basin component of the Roper Seaway. Trace element data reveal that the basinal waters were suboxic to anoxic with episodes of euxinia. This onset of euxinia occurred during an influx of organic matter, this flux may have been greater than the contemporary reactive Fe flux, allowing H_2S to build up. Considering that euxinic conditions require the S/Fe ratio to be greater than 2, and that the Velkerri Formation geochemistry imply high levels of reactive Fe, significant sulphate must have been available for sulphate reduction. This implies that sufficient levels of atmospheric O_2 were available to drive the oxidative continental weathering of sulphides. Furthermore, although deep-water suboxic to anoxic conditions prevailed, the presence of negative Ce anomalies at the very least, implies active redox cycling of Ce, and most likely points towards oxygenated shallow water.

As major and trace element data support long-lived suboxic to anoxic deep-water, the high organic content of the middle Velkerri Formation cannot be explained through redox-controlled enhancement in preservation potential, nor through climate change. However, the high TOC contents can be reconciled due to its covariation with both major element and high-field strength element abundances, and 143Nd/144Nd ratios, with a transition in sediment provenance to more mafic sources. These mafic sources would have resulted in increased phosphorus delivery, potentially resulting in enhanced primary productivity.

Acknowledgements

GMC, DE and AM publish with the permission of the CEO, Geoscience Australia. We would like to acknowledge the support of the laboratory staff at Geoscience Australia. The Northern Territory Geological Survey (NTGS) and the staff of the Darwin Core Library are thanked for facilitating access to the core. Clint Scott, Andrey Bekker and Marcus Kunzmann are thanked for their reviews which improved this manuscript immeasurably. Steve Abbott, Chris Boreham and David Huston are thanked for their review of the preliminary manuscript. GMC's and ASC's contribution forms TRaX Record #348.

Appendix A. Supplementary data

Supplementary data to this article can be found online at http://dx.doi.org/10.1016/j.chemgeo.2016.06.025.

References

Abbott, J.G., 1997. Geology of the Upper Hart River Area, Eastern Ogilvie Mountains, Yukon Territory (116A/10, 116A/11).

Abbott, S.T., Sweet, I.P., 2000. Tectonic control on third-order sequences in a siliciclastic ramp-style basin: an example from the Roper Superbasin (Mesoproterozoic), northern Australia. Aust. J. Earth Sci. 47 (3), 637–657.

Abbott, S. et al., 2001. Roper Region: Urapunga and Roper River Special SD 53–10 & 11, 1: 250000 Geological Map Series Explantory Notes. Northern Territory Geological Survey, Darwin.

Algeo, T.J., Maynard, J.B., 2004. Trace-element behavior and redox facies in core shales of Upper Pennsylvanian Kansas-type cyclothems. Chem. Geol. 206 (3–4), 289–318.

Anbar, A.D., et al., 2007. A whiff of oxygen before the great oxidation event? Science 317 (5846), 1903–1906.

Anderson, R.F., Fleisher, M.Q., LeHuray, A.P., 1989. Concentration, oxidation state, and particulate flux of uranium in the Black Sea. Geochim. Cosmochim. Acta 53 (9), 2215–2224.

Barnes, C.E., Cochran, J.K., 1993. Uranium geochemistry in estuarine sediments: controls on removal and release processes. Geochim. Cosmochim. Acta 57 (3), 555–569.

Barovich, K.M., Foden, J., 2000. A Neoproterozoic flood basalt province in southern-central Australia: geochemical and Nd isotope evidence from basin fill. Precambrian Res. 100 (1–3), 213–234.

Bau, M., Dulski, P., 1996. Distribution of yttrium and rare-earth elements in the Penge and Kuruman iron-formations, Transvaal Supergroup, South Africa. Precambrian Res. 79 (1–2), 37–55.

Bekker, A., et al., 2010. Iron formation: the sedimentary product of a complex interplay among mantle, tectonic, oceanic, and biospheric processes. Econ. Geol. 105 (3), 467–508.

Betts, P.G., Giles, D., 2006. The 1800–1100 Ma tectonic evolution of Australia. Precambrian Res. 144 (1–2), 92–125.

Blewett, R.S., Black, L.P., 1998. Structural and temporal framework of the Coen Region, north Queensland: implications for major tectonothermal events in east and north Australia. Aust. J. Earth Sci. 45 (4), 597–609.

Blewett, R.S., et al., 1997. Coen Region. In: Bain, J.H.C., Draper, J.J. (Eds.), North Queensland Geology. Australian Geological Survey Organisation, pp. 117–158.

Blewett, R.S., et al., 1998. U/Pb zircon and Sm/Nd geochronology of the Mesoproterozoic of North Queensland: implications for a Rodinian connection with the Belt supergroup of North America. Precambrian Res. 89 (3–4), 101–127.

Bradley, D.C., 2008. Passive margins through earth history. Earth Sci. Rev. 91 (1–4), 1–26.

Brasier, M.D., Lindsay, J.F., 1998. A billion years of environmental stability and the emergence of eukaryotes: new data from northern Australia. Geology 26 (6), 555–558.

Breit, G.N., Wanty, R.B., 1991. Vanadium accumulation in carbonaceous rocks: a review of geochemical controls during deposition and diagenesis. Chem. Geol. 91 (2), 83–97.

Bruno, J., De Pablo, J., Duro, L., Figuerola, E., 1995. Experimental study and modeling of the U(VI)–Fe(OH)3 surface precipitation/coprecipitation equilibria. Geochim. Cosmochim. Acta 59 (20), 4113–4123.

Buick, R., Des Marais, D.J., Knoll, A.H., 1995. Stable isotopic compositions of carbonates from the Mesoproterozoic Bangemall group, northwestern Australia. Chem. Geol. 123 (1–4), 153–171.

Calvert, S.E., Pedersen, T.F., 1993. Marine sediments, burial, pore water chemistry, microbiology and diagenesis geochemistry of recent oxic and anoxic marine sediments: implications for the geological record. Mar. Geol. 113 (1), 67–88.

Canfield, D.E., 1998. A new model for Proterozoic ocean chemistry. Nature 396 (6710), 450–453.

Cawood, P.A., Hawkesworth, C.J., 2014. Earth's middle age. Geology 42 (6), 503–506.

Colin, C., et al., 2006. Evolution of weathering patterns in the Indo-Burman Ranges over the last 280 kyr: effects of sediment provenance on $^{87}Sr/^{86}Sr$ ratios tracer. Geochem. Geophys. Geosyst. 7 (3) (n/a-n/a).

Collier, R.W., 1985. Molybdenum in the Northeast Pacific Ocean. Limnol. Oceanogr. 30 (6), 1351–1354.

Condie, K.C., Des Marais, D.J., Abbott, D., 2001. Precambrian superplumes and supercontinents: a record in black shales, carbon isotopes, and paleoclimates? Precambrian Res. 106 (3–4), 239–260.

Cox, G.M., et al., 2016. Continental flood basalt weathering as a trigger for Neoproterozoic Snowball Earth. Earth Planet. Sci. Lett. 446, 88–99.

Crick, I.H., Boreham, C.J., Cook, A.C., Powell, T.G., 1988. Petroleum geology and geochemistry of Middle Proterozoic McArthur Basin, Northern Australia: assessment of source rock potential. AAPG Bull. 72 (12), 1495–1514.

Donnelly, T.H., Crick, I.H., 1988. Depositional environment of the middle proterozoic velkerri formation in Northern Australia: geochemical evidence. Precambrian Res. 42 (1–2), 165–172.

Dumoulin, J.A., Slack, J.F., Whalen, M.T., Harris, A.G., 2011. Depositional setting and geochemistry of phosphorites and metalliferous black shales in the Carboniferous-Permian Lisburne Group, Northern Alaska. USGS Professional Paper 1776C, Reston, VA.

Elderfield, H., Greaves, M.J., 1981. Negative cerium anomalies in the rare earth element patterns of oceanic ferromanganese nodules. Earth Planet. Sci. Lett. 55 (1), 163–170.

Elderfield, H., Hawkesworth, C.J., Greaves, M.J., Calvert, S.E., 1981. Rare earth element geochemistry of oceanic ferromanganese nodules and associated sediments. Geochim. Cosmochim. Acta 45 (4), 513–528.

Erickson, B.E., Helz, G.R., 2000. Molybdenum(VI) speciation in sulfidic waters: stability and lability of thiomolybdates. Geochim. Cosmochim. Acta 64 (7), 1149–1158.

Ernst, R.E., Wingate, M.T.D., Buchan, K.L., Li, Z.X., 2008. Global record of 1600–700 Ma Large Igneous Provinces (LIPs): implications for the reconstruction of the proposed Nuna (Columbia) and Rodinia supercontinents. Precambrian Res. 160, 159–178.

Fagel, N., 2007. Chapter four clay minerals, deep circulation and climate. In: Claude, H.M., Anne De, V. (Eds.), Developments in Marine Geology. Elsevier, pp. 139–184.

Fedo, C.M., Wayne Nesbitt, H., Young, G.M., 1995. Unraveling the effects of potassium metasomatism in sedimentary rocks and paleosols, with implications for paleoweathering conditions and provenance. Geology 23 (10), 921–924.

Firdaus, M.L., Minami, T., Norisuye, K., Sohrin, Y., 2011. Strong elemental fractionation of Zr–Hf and Nb–Ta across the Pacific Ocean. Nat. Geosci. 4 (4), 227–230.

Foster, D.A., Ehlers, K., 1998. $^{40}Ar–^{39}Ar$ thermochronology of the southern Gawler Craton, Australia: implications for Mesoproterozoic and Neoproterozoic tectonics of East Gondwana and Rodinia. J. Geophys. Res. Solid Earth 103 (B5), 10177–10193.

Gilleaudeau, G.J., et al., 2016. Oxygenation of the mid-Proterozoic atmosphere: clues from chromium isotopes in carbonates. Geochem. Perspect. Lett. 2 (0), 178–187.

Gingele, F.X., Müller, P.M., Schneider, R.R., 1998. Orbital forcing of freshwater input in the Zaire Fan area—clay mineral evidence from the last 200 kyr. Palaeogeogr. Palaeoclimatol. Palaeoecol. 138 (1–4), 17–26.

Goldstein, S.L., O'Nions, R.K., Hamilton, P.J., 1984. A Sm–Nd isotopic study of atmospheric dusts and particulates from major river systems. Earth Planet. Sci. Lett. 70 (2), 221–236.

Hall, L.S., et al., 2016. Cooper Basin source rock geochemistry: regional hydrocarbon prospectivity of the Cooper Basin, Part 2. Record 2016/06. Geoscience Australia, Canberra.

Hartnett, H.E., Keil, R.G., Hedges, J.I., Devol, A.H., 1998. Influence of oxygen exposure time on organic carbon preservation in continental margin sediments. Nature 391 (6667), 572–575.

Hedges, J.I., Keil, R.G., 1995. Sedimentary organic matter preservation: an assessment and speculative synthesis. Mar. Chem. 49 (2–3), 81–115.

Horton, F., 2015. Did phosphorus derived from the weathering of large igneous provinces fertilize the Neoproterozoic ocean? Geochem. Geophys. Geosyst. 16, 1723–1738.

Jackson, M.J., Raiswell, R., 1991. Sedimentology and carbon-sulphur geochemistry of the Velkerri Formation, a mid-Proterozoic potential oil source in northern Australia. Precambrian Res. 54 (1), 81–108.

Jackson, M.J., Powell, T.G., Summons, R.E., Sweet, I.P., 1986. Hydrocarbon shows and petroleum source rocks in sediments as old as 1.7 [times] 109 years. Nature 322 (6081), 727–729.

Jackson, M.J., Muir, M.D., Plumb, K.A., 1987. In: Energy, D.o.R.a. (Ed.), Geology of the southern McArthur Basin, Northern Territory. Bureau of Mineral Resouces, Geology and Geophysics, Canberra.

Jackson, M.J., Sweet, I.P., Page, R.W., Bradshaw, B.E., 1999. Integrated Basin Analysis of the Isa Superbasin using Seismic, Well-log and Geopotential Data. Australian Geological Survey Organisation, Canberra.

Javaux, E.J., Knoll, A.H., Walter, M.R., 2001. Morphological and ecological complexity in early eukaryotic ecosystems. Nature 412 (6842), 66–69.

Javaux, E.J., Knoll, A.H., Walter, M.R., 2004. TEM evidence for eukaryotic diversity in mid-Proterozoic oceans. Geobiology 2 (3), 121–132.

Johnston, D.T., et al., 2010. An emerging picture of Neoproterozoic ocean chemistry: insights from the Chuar Group, Grand Canyon, USA. Earth Planet. Sci. Lett. 290 (1–2), 64–73.

Kah, L.C., Sherman, A.G., Narbonne, G.M., Knoll, A.H., Kaufman, A.J., 1999. $\delta^{13}C$ stratigraphy of the Proterozoic Bylot Supergroup, Baffin Island, Canada: implications for regional lithostratigraphic correlations. Can. J. Earth Sci. 36 (3), 313–332.

Kasting, J.F., Ono, S., 2006. Palaeoclimates: the first two billion years. Philos. Trans. R. Soc. Lond. Ser. B Biol. Sci. 361 (1470), 917–929.

Kendall, B., Creaser, R.A., Gordon, G.W., Anbar, A.D., 2009. Re–Os and Mo isotope systematics of black shales from the Middle Proterozoic Velkerri and Wollogorang Formations, McArthur Basin, northern Australia. Geochim. Cosmochim. Acta 73 (9), 2534–2558.

Kennedy, M.J., Pevear, D.R., Hill, R.J., 2002. Mineral surface control of organic carbon in black shale. Science 295 (5555), 657–660.

Klinkhammer, G.P., Palmer, M.R., 1991. Uranium in the oceans: where it goes and why. Geochim. Cosmochim. Acta 55 (7), 1799–1806.

Kunzmann, M., Halverson, G.P., Scott, C., Minarik, W.G., Wing, B.A., 2015. Geochemistry of Neoproterozoic black shales from Svalbard: implications for oceanic redox conditions spanning Cryogenian glaciations. Chem. Geol. 417, 383–393.

Langmuir, D., 1978. Uranium solution-mineral equilibria at low temperatures with applications to sedimentary ore deposits. Geochim. Cosmochim. Acta 42 (6 PART A), 547–569.

Lewan, M.D., Maynard, J.B., 1982. Factors controlling enrichment of vanadium and nickel in the bitumen of organic sedimentary rocks. Geochim. Cosmochim. Acta 46 (12), 2547–2560.

Li, Z.X., et al., 2008. Assembly, configuration, and break-up history of Rodinia: a synthesis. Precambrian Res. 160 (1–2), 179–210.

Lindsay, J.F., 2001. Basin dynamics and mineralisation, McArthur Basin, northern Australia. Aust. J. Earth Sci. 48 (5), 703–720.

Lyons, T.W., Anbar, A.D., Severmann, S., Scott, C., Gill, B.C., 2009a. Tracking euxinia in the Ancient Ocean: a multiproxy perspective and Proterozoic case study. Annu. Rev. Earth Planet. Sci. 37 (1), 507–534.

Lyons, T.W., Reinhard, C.T., Scott, C., 2009b. Redox redux. Geobiology 7 (5), 489–494.

Lyons, T.W., Reinhard, C.T., Planavsky, N.J., 2014. The rise of oxygen in Earth/'s early ocean and atmosphere. Nature 506 (7488), 307–315.

Mayer, L.M., 1994. Surface area control of organic carbon accumulation in continental shelf sediments. Geochim. Cosmochim. Acta 58 (4), 1271–1284.

McManus, J., Berelson, W.M., Klinkhammer, G.P., Hammond, D.E., Holm, C., 2005. Authigenic uranium: relationship to oxygen penetration depth and organic carbon rain. Geochim. Cosmochim. Acta 69 (1), 95–108.

Meyer, K.M., Kump, L.R., 2008. Oceanic euxinia in Earth history: causes and consequences. Annu. Rev. Earth Planet. Sci. 36 (1), 251–288.

Mulder, J.A., Halpin, J.A., Daczko, N.R., 2015. Mesoproterozoic Tasmania: witness to the east Antarctica–Laurentia connection within Nuna. Geology 43 (9), 759–762.

Müller, P.J., Suess, E., 1979. Productivity, sedimentation rate, and sedimentary organic matter in the oceans—I. Organic carbon preservation. Deep Sea Res. Part A 26 (12), 1347–1362.

Nagender Nath, B., Roelandts, I., Sudhakar, M., Plger, W.L., Balaram, V., 1994. Cerium anomaly variations in ferromanganese nodules and crusts from the Indian Ocean. Mar. Geol. 120 (3–4), 385–400.

Nance, W.B., Taylor, S.R., 1976. Rare earth element patterns and crustal evolution — I. Australian post-Archean sedimentary rocks. Geochim. Cosmochim. Acta 40 (12), 1539–1551.

Nesbitt, H.W., Young, G.M., 1982. Early Proterozoic climates and plate motions inferred from major element chemistry of lutites. Nature 299 (5885), 715–717.

Peacor, D.R., Coveney, R.M., Zhao, G., 2000. Authigenic illite and organic matter: the principal hosts of vanadium in the Mecca Quarry Shale at Velpen, Indiana. Clay Clay Miner. 48 (3), 311–316.
Pedersen, T.F., Calvert, S.E., 1990. Anoxia vs productivity; what controls the formation of organic-carbon-rich sediments and sedimentary rocks? AAPG Bull. 74 (4), 454–466.
Pi, D.-H., Liu, C.-Q., Shields-Zhou, G.A., Jiang, S.-Y., 2013. Trace and rare earth element geochemistry of black shale and kerogen in the early Cambrian Niutitang Formation in Guizhou province, South China: constraints for redox environments and origin of metal enrichments. Precambrian Res. 225, 218–229.
Pietsch, B.A. et al., 1991. Bauhinia Downs, Northern Territory (Second Edition). 1:250,000 geological map series explanatory notes, SE 53-03, Northern Territory Geological Survey, Darwin.
Pisarevsky, S.A., Elming, S.-Å., Pesonen, L.J., Li, Z.-X., 2014. Mesoproterozoic paleogeography: supercontinent and beyond. Precambrian Res. 244, 207–225.
Planavsky, N.J., et al., 2014. Low Mid-Proterozoic atmospheric oxygen levels and the delayed rise of animals. Science 346 (6209), 635–638.
Plumb, K.A., Roberts, H.G., 1992. The geology of Arnhem Land, Northern Territory. Mineral Provinces 15Record 1992/55. Bureau of Mineral Resources, Australia.
Plumb, K.A., Wellman, P., 1987. McArthur Basin, Northern Territory: mapping of deep troughs using gravity and magnetic anomalies. BMR J. Aust. Geol. Geophys. 10 (3), 243–251.
Powell, T.G., et al., 1987. Petroleum geology and geochemsitry. Middle Proterozoic McArthur Basin. Bureau of Mineral Resources.
Rawlings, D.J., 1999. Stratigraphic resolution of a multiphase intracratonic basin system: the McArthur Basin, northern Australia. Aust. J. Earth Sci. 46 (5), 703–723.
Rawlings, D.J., et al., 2004. The 2002 Southern McArthur Basin Seismic Reflection Survey. Geoscience Australia, Canberra.
Reinhard, C.T., et al., 2013. Proterozoic ocean redox and biogeochemical stasis. Proc. Natl. Acad. Sci. 110 (14), 5357–5362.
Roberts, N.M.W., 2013. The boring billion? – Lid tectonics, continental growth and environmental change associated with the Columbia supercontinent. Geosci. Front. 4 (6), 681–691.
Rogers, J.J.W., Santosh, M., 2002. Configuration of Columbia, a Mesoproterozoic supercontinent. Gondwana Res. 5 (1), 5–22.
Rooney, A.D., et al., 2014. Re–Os geochronology and coupled Os–Sr isotope constraints on the Sturtian snowball Earth. Proc. Natl. Acad. Sci.
Schneider, R.R., Price, B., Müller, P.J., Kroon, D., Alexander, I., 1997. Monsoon related variations in Zaire (Congo) sediment load and influence of fluvial silicate supply on marine productivity in the east equatorial Atlantic during the last 200,000 years. Paleoceanography 12 (3), 463–481.
Scott, C., Lyons, T.W., 2012. Contrasting molybdenum cycling and isotopic properties in euxinic versus non-euxinic sediments and sedimentary rocks: Refining the paleoproxies. Chem. Geol. 324–325, 19–27.
Scott, C., et al., 2008. Tracing the stepwise oxygenation of the Proterozoic ocean. Nature 452 (7186), 456–459.
Shen, Y., Knoll, A.H., Walter, M.R., 2003. Evidence for low sulphate and anoxia in a mid-Proterozoic marine basin. Nature 423 (6940), 632–635.
Slack, J.F., Grenne, T., Bekker, A., Rouxel, O.J., Lindberg, P.A., 2007. Suboxic deep seawater in the late Paleoproterozoic: evidence from hematitic chert and iron formation related to seafloor-hydrothermal sulfide deposits, central Arizona, USA. Earth Planet. Sci. Lett. 255 (1–2), 243–256.
Slack, J.F., Selby, D., Dumoulin, J.A., 2015. Hydrothermal, biogenic, and seawater components in metalliferous black shales of the Brooks Range, Alaska: synsedimentary metal enrichment in a carbonate ramp setting. Econ. Geol. 110 (3), 653–675.
Southgate, P.N., et al., 2000. Chronostratigraphic basin framework for Palaeoproterozoic rocks (1730–1575 Ma) in northern Australia and implications for base-metal mineralisation. Aust. J. Earth Sci. 47 (3), 461–483.
Sperling, E.A., et al., 2014. Redox heterogeneity of subsurface waters in the Mesoproterozoic ocean. Geobiology 12 (5), 373–386.
Sperling, E.A., et al., 2015. Statistical analysis of iron geochemical data suggests limited late Proterozoic oxygenation. Nature 523 (7561), 451–454.
Spikings, R.A., Foster, D.A., Kohn, B.P., Lister, G.S., 2001. Post-orogenic (<1500 Ma) thermal history of the Proterozoic Eastern Fold Belt, Mount Isa Inlier, Australia. Precambrian Res. 109 (1–2), 103–144.
Spikings, R.A., Foster, D.A., Kohn, B.P., Lister, G.S., 2002. Post-orogenic (<1500 Ma) thermal history of the Palaeo-Mesoproterozoic, Mt. Isa province, NE Australia. Tectonophysics 349 (1–4), 327–365.
Stribrny, B., Urban, H., 1989. Classification of Sedimentary Rocks in the Black Shale Series Based on Their Normative Mineral Compositions. International Geological Congress, Washington, D.C., pp. 190–191 Abstracts.
Sun, S.-S., McDonough, W.F., 1989. Chemical and isotopic systematics of oceanic basalts: implications for mantle composition and processes. Magmatism in the Ocean Basins 42. Geological Society, London, Special Publications, p. 42 (313–345 pp.).
Sweet, I.P., Jackson, M.J., 1986. BMR Stratigraphic Drilling in the Roper Group, Northern Territory. Bureau of Mineral Resources, Geology and Geophysics, Canberra.
Takeno, N., 2005. Atlas of Eh–pH Diagrams — Intercomparison of Thermodynamic Databases. National Institute of Advanced Industrial Science and Technology.
Taylor, S.R., McLennan, S.M., 1985. The Continental Crust: Its Composition and Evolution. Blackwell, Oxford (312 pp.).
Taylor, S.R., McLennan, S.M., 1995. The geochemical evolution of the continental crust. Rev. Geophys. 33 (2), 241–265.
Thorkelson, D.J., et al., 2005. Early and Middle Proterozoic evolution of Yukon, Canada. Can. J. Earth Sci. 42.
Tribovillard, N., Algeo, T.J., Lyons, T., Riboulleau, A., 2006. Trace metals as paleoredox and paleoproductivity proxies: an update. Chem. Geol. 232 (1–2), 12–32.
Tyrrell, T., 1999. The relative influences of nitrogen and phosphorus on oceanic primary production. Nature 400 (6744), 525–531.
Volk, H., Dutkiewicz, A., George, S., Ridley, J., 2003. Oil migration in the Middle Proterozoic Roper Superbasin,Australia: evidence from oil inclusions and their geochemistries. J. Geochem. Explor. 78–79 (0), 437–441.
Wanty, R.B., Goldhaber, M.B., 1992. Thermodynamics and kinetics of reactions involving vanadium in natural systems: accumulation of vanadium in sedimentary rocks. Geochim. Cosmochim. Acta 56 (4), 1471–1483.
Warren, J.K., George, S.C., Hamilton, P.J., Tingate, P., 1998. Proterozoic source rocks; sedimentology and organic characteristics of the Velkerri Formation, Northern Territory, Australia. AAPG Bull. 82 (3), 442–463.
White, A.F., Brantley, S.L., 1995. Chemical weathering rates of silicate minerals; an overview. Rev. Mineral. Geochem. 31, 1–22.
Zhang, S., et al., 2012. Pre-Rodinia supercontinent Nuna shaping up: a global synthesis with new paleomagnetic results from North China. Earth Planet. Sci. Lett. 353–354, 145–155.
Zhang, S., et al., 2016. Sufficient oxygen for animal respiration 1400 million years ago. Proc. Natl. Acad. Sci. 113 (7), 1731–1736.
Zhu, S., et al., 2016. Decimetre-scale multicellular eukaryotes from the 1.56-billion-year-old Gaoyuzhuang Formation in North China. Nat. Commun. 7.